High Contrast Stellar Observations within the Diffraction Limit at the Palomar Hale Telescope

B. Mennesson[a], C. Hanot[b], E.Serabyn[a], S.R.Martin[a], K.Liewer[a], F.Loya[a] and D.Mawet[a]

[a]Jet Propulsion Laboratory, California Institute of Technology, 4800 Oak Grove Drive, Pasadena CA 91109-8099;

[b]AEOS, University of Liège, Allée du 6 Août, 17 Bât B5c, 4000 Liège, Belgium

ABSTRACT

We report on high-accuracy, high-resolution (< 20mas) stellar measurements obtained in the near infrared ($\simeq$ 2.2 microns) at the Palomar 200 inch telescope using two elliptical (3 m x 1.5 m) sub-apertures located 3.4 m apart. Our interferometric coronagraph, known as the "Palomar Fiber Nuller" (PFN), is located downstream of the Palomar adaptive optics (AO) system and recombines the two separate beams into a common single-mode fiber. The AO system acts as a "fringe tracker", maintaining the optical path difference (OPD) between the beams around an adjustable value, which is set to the central dark interference fringe. AO correction ensures high efficiency and stable injection of the beams into the single-mode fiber. A chopper wheel and a fast photometer are used to record short (< 50ms per beam) interleaved sequences of background, individual beam and interferometric signals. In order to analyze these chopped null data sequences, we developed a new statistical method, baptized "Null Self-Calibration" (NSC), which provides astrophysical null measurements at the 0.001 level, with 1 σ uncertainties as low as 0.0003. Such accuracy translates into a dynamic range greater than 1000:1 within the diffraction limit, demonstrating that the approach effectively bridges the traditional gap between regular coronagraphs, limited in angular resolution, and long baseline visibility interferometers, whose dynamic range is restricted to $\simeq$ 100:1. As our measurements are extremely sensitive to the brightness distribution very close to the optical axis, we were able to constrain the stellar diameters and amounts of circumstellar emission for a sample of very bright stars. With the improvement expected when the PALM-3000 extreme AO system comes on-line at Palomar, the same instrument now equipped with a state of the art low noise fast read-out near IR camera, will yield 10^{-4} to 10^{-3} contrast as close as 30 mas for stars with K magnitude brighter than 6. Such a system will provide a unique and ideal tool for the detection of young (<100 Myr) self-luminous planets and hot debris disks in the immediate vicinity (0.1 to a few AUs) of nearby (< 50pc) stars.

Keywords: infrared: stars — instrumentation: coronagraphs, interferometers — stars: circumstellar matter — stars: individual (α Boo, Vega, ρ Per)

1. INTRODUCTION

Near infrared coronagraphs working with current-generation AO systems mounted on large (diameter D > 5 m) ground based telescopes have inner working angles limited to 300 mas or more. In the case of traditional Lyot coronagraphs,[1,2] this limit is directly fixed by the size of the occulting focal plane mask. In the case of phase coronagraphs, the practical resolution limit for deep (say 10^{-4} contrast or better) imaging at near infrared wavelengths is also $\simeq$ 5 to 10 λ/D because of residual wavefront corrugations.[3] Operation closer to the axis ($\simeq \lambda/D$) is only possible with extreme AO, such as is demonstrated by observations with a 1.5 m diameter well corrected subaperture.[4] Future coronagraphs such as SPHERE[5] and GPI,[6] using extreme AO on large 8 m telescopes, will soon allow improved performance close to the optical axis. However, even with these next generation instruments, high contrast in the near infrared will only be available at $\simeq$ 3 λ/D, i.e at least 100 mas away from the optical axis. Near infrared interferometry operates in a very different angular regime. The resolution ranges from 20 to 30 mas when using sub-apertures of 5 to 8m telescopes, to a mas or better using

Further author information: (Send correspondence to BM)
E-mail: bertrand.mennesson@jpl.nasa.gov, Telephone: 1 818 354 0494

Ground-based and Airborne Instrumentation for Astronomy III, edited by Ian S. McLean, Suzanne K. Ramsay, Hideki Takami, Proc. of SPIE Vol. 7735, 773511 · © 2010 SPIE · CCC code: 0277-786X/10/$18 · doi: 10.1117/12.857633

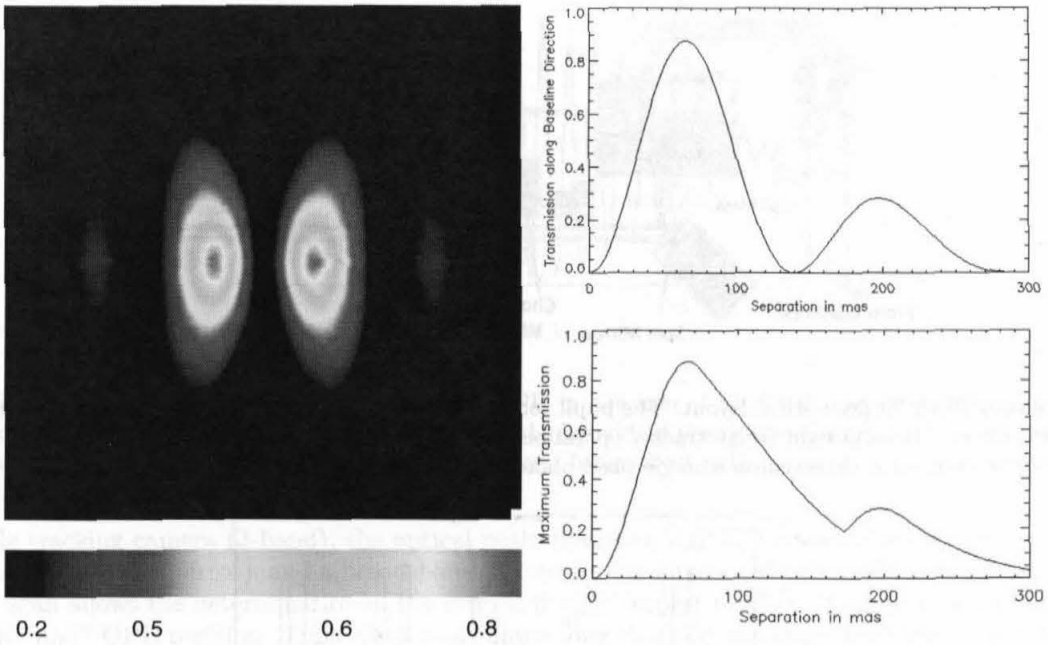

Figure 1. Left: PFN sky transmission over 0.6" x 0.6" field of view, assuming a "horizontal" 3.41 m baseline separating two elliptical sub-apertures (3 m x 1.5 m). Top right: PFN transmission vs separation, along baseline direction. Bottom right: Maximum transmission versus baseline rotation angle, as a function of separation.

separate telescopes (e.g. the recent beautiful CHARA MIRC infrared images of the transiting disk in the ϵ Aurigae system[7]).

The fiber nulling interferometric approach was validated in the laboratory, using monochromatic visible light[8] initially, and then broad-band near infrared light in H[9] and K[10] band. Its principle is to combine two spatially separated beams into a common single-mode fiber while maintaining a π differential phase shift between the beams. Since the individual wavefronts of the two sub-apertures are spatially filtered by the fiber, the accessible cancellation level is primarily fixed by the residual OPD between the two sub-apertures, and not by the individual wavefront errors.[11] This fundamental property allows the occurrence of frequent deep quasi-instantaneous (a few ms) nulls, even when the individual stellar wavefronts are extracted from a large telescope characterized by the Strehl ratio of current AO systems ($\simeq$ 70% at K band). Nulling two sub-apertures of diameter d separated by a distance b, the 50% transmission point corresponds to an off-axis separation $\lambda/4b$, while the field of view FWHM is limited to $\simeq \lambda/d$. The Palomar Fiber Nuller (PFN) observes in the K band and uses two elliptical 3m x 1.5m sub-apertures located a distance b=3.4 m apart. Its sky transmission is represented in figure 1, showing a 50% transmission point at 33 mas -to be compared with the 200 mas FWHM sub-aperture field of view, and the full telescope 90 mas PSF. In essence, a fiber nuller system offers a natural complement to a traditional coronagraph: from a resolution standpoint, it starts working where a regular coronagraph stops and vice versa.

The PFN first generation system depicted here was built as a sky technological demonstrator and restricted to the observations of *very bright stars*. After a short presentation of the PFN optical set-up and observing methodology, we discuss the data reduction strategy specifically developed for the PFN. Finally we present the results obtained on nine bright stars, for which accurate sizes are determined, and excess circumstellar emission is characterized down to the 0.1% level.

2. OPTICAL SET-UP AND METHODOLOGY

A full description of the PFN hardware is given in a recent fiber nuller design paper.[10] The PFN (figure 2) is mounted on a stand alone 4' x 2' bread-board inserted downstream of the Palomar AO system, in place of the

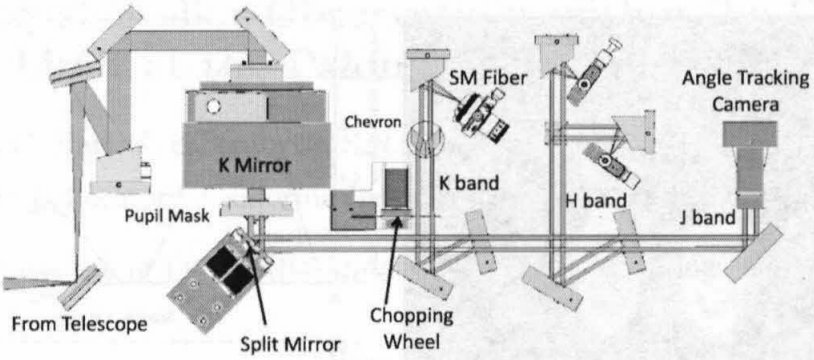

Figure 2. Palomar Fiber Nuller optical layout. The pupil rotator (K-mirror) rotates the image of the fixed pupil mask on the telescope primary. H band light fringe tracker operational in the laboratory, but not tested on the sky. The K-band single-mode fiber's output is detected on a single pixel photometer (unshown). See text for details.

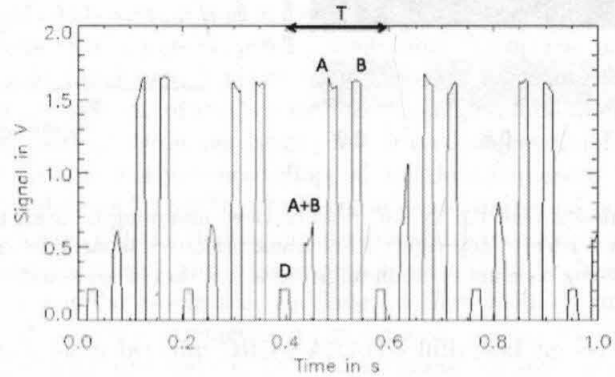

Figure 3. Chopped signal recorded on α Her. Cycle period: T=186 ms. Five successive cycles are shown, each with alternate measurements of dark ("D"), interferometric ("A+B") and individual ("A", "B") beam intensities. Parts of a cycle located around beam transitions are discarded.

standard near infrared PHARO camera. Under average seeing conditions and for the bright stars considered here, the AO system[12] delivers to the PFN an input wavefront with a typical 200 to 250 nm rms figure in the K band. The AO system can be thought at as a first order fringe tracker, maintaining the relative phase difference between the 2 beams to be nulled. After the AO bench, a fold mirror delivers the f/16 converging beam to the PFN. On the PFN bench, after collimation, the stellar beam first goes through a "K-mirror" used to rotate the pupil with respect to the PFN. The beam subsequently goes through a mask with two elliptical holes defining the fiber nuller sub-apertures (3 m x 1.5 m equivalent sizes on the primary) and interferometric baseline (3.41 m equivalent length on the primary). A split mirror allows independent control of the beams optical paths and directions. A dichroic inserted in each of the 2 sub-beams (denoted "A" and "B") provides angle tracking in the J band. The K band science beams go through a spatial chopper providing alternate measurements of dark ("D"), including detector and background contributions), interferometric ("A+B") and individual (A, B) beam intensities (figure 3) over cycles of $\simeq$ 200 ms.

A chevron shaped piece of infrasil glass brings the 2 science beams closer to each other (for better injection efficiency into the fiber, typically 40%) and introduces a constant differential glass thickness between the beams. This differential thickness is set to the value minimizing the wideband null over the K band, using same principle as previously demonstrated in N-band.[13] Finally, a common off-axis parabola is used for recombination, injecting the two beams into a single-mode fiber. The fiber output is then re-imaged onto a fast single-pixel infrared (InGaAs) photometer. For a given target, the observations start by optimizing the flux injected into the fiber for each of the sub-beams using the two tip-tilt mirrors of the PFN. While the stellar position is maintained

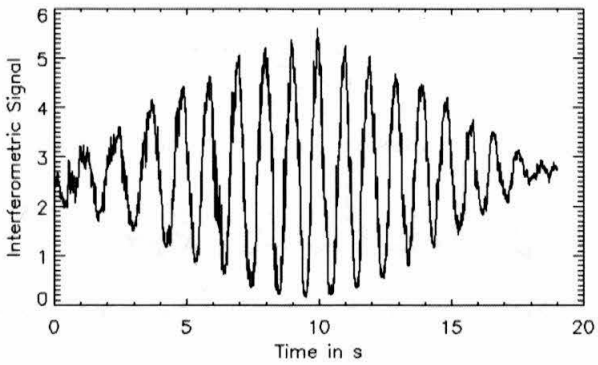

Figure 4. Fringe scan recorded on α Her by varying the OPD in one arm of the PFN (raw data sampled every 10 ms). AO correction and J-band angle tracking typically stabilize the individual beams photometry at the 3-10% rms level over five minutes. Such interferograms are used to locate the central fringe (best null) position

on the angle tracking camera (J-band), the optical path difference (OPD) between the beams is scanned via a PZT driven mirror (split mirror), and a broad-band interferogram is recorded on the K-band detector (figure 4). This fringe scan allows the determination of the central fringe (deepest null) position and the instrument phase is set at this "null" OPD position. Typically 1 to 5 minute long chopped sequences are then recorded per target, alternating rapidly between individual beams, dark and null signal measurements. In the cases of α Her, β Peg and Vega, the K-mirror was rotated to provide different baseline orientations on the sky and to begin to test the baseline rotation and signal modulation aspects.

3. PFN'S OBSERVABLE AND DATA REDUCTION

Given a series of $\simeq$ 200 ms long cycles, each consisting of successive Dark (D), interferometric (A+B) and individual (A,B) measurements, one computes the quantities:

$$\hat{I}_N(t) = (A+B)(t) - \hat{D}(t) \quad (1)$$

$$\hat{I}_1(t) = \hat{A}(t) - \hat{D}(t) \quad (2)$$

$$\hat{I}_2(t) = \hat{B}(t) - \hat{D}(t) \quad (3)$$

$$\hat{I}_P(t) = \hat{I}_1(t) + \hat{I}_2(t) + 2\sqrt{\hat{I}_1(t).\hat{I}_2(t)} \quad (4)$$

$$N_{obs}(t) = \frac{\hat{I}_N(t)}{\hat{I}_P(t)} \quad (5)$$

Within a given cycle, the quantity (A+B)(t) is the instantaneous interferometric signal (close to null) recorded every 2 ms, while $\hat{A}$(t), $\hat{B}$(t) and $\hat{D}$(t) are the measured averages of A, B and D over the same cycle. $\hat{I}_N(t)$, $\hat{I}_P(t)$, $\hat{I}_1(t)$ and $\hat{I}_2(t)$ serve as best estimates of the instantaneous null, peak and individual signals $I_N(t)$, $I_P(t)$, $I_1(t)$ and $I_2(t)$ at the time of an (A+B) interferometric measurement. $N_{obs}(t)$ is the observed normalized instantaneous null depth, based on the measured chopped signals.

In the case of the PFN, the two beams are injected into a *common* single-mode fiber. Neglecting any differential polarization effects in the beam train, the recorded interferometric signal (A+B)(t) can be approximated by:

$$(A+B)(t) = I_1(t) + I_1(t) + 2|V|.\sqrt{I_1(t)I_2(t)}.cos(\Delta\phi(t) + \phi_V) + D(t) \quad (6)$$

Where $|V|$ is the complex modulus of the source visibility, ϕ_V its phase, and $\phi(t)$ the instantaneous differential phase between the beams, maintained close to π. Using equations 1 to 6, $N_{obs}(t)$ can be modeled as:

$$N_{model}(t) = \frac{I_1(t) + I_2(t) + 2|V|.\sqrt{I_1(t)I_2(t)}.cos(\phi(t) + \phi_V)}{\hat{I}_P(t)}) + \frac{(D(t) - \hat{D}(t))}{\hat{I}_P(t)} \quad (7)$$

All PFN data are analyzed using this expression. In the deep null regime ($N_{obs}(t) << 1$), it reduces to:

$$N_{model}(t) = (N^{as} + \frac{(dI)^2(t)}{4} + \frac{(\Delta\phi)^2(t)}{4}).(\frac{I_P(t)}{\hat{I}_P(t)}) + \frac{(D(t) - \hat{D}(t))}{\hat{I}_P(t)} \quad (8)$$

where N^{as} is the target astrophysical null depth, a simple function of the object complex visibility V at the PFN's baseline:

$$N^{as} = \frac{1 - |V|}{1 + |V|} \quad (9)$$

Equation (8) shows that in addition to the constant astrophysical contribution N^{as}, the observed null depth includes some time variable instrumental terms. The main contributors (always positive) are the beam intensity mismatch term in $(dI)^2$(t), - with dI defined as $dI(t) = [I_1(t) - I_2(t)]/[I_1(t) + I_2(t)]$ -, and the phase mismatch term in $(\Delta\phi)^2(t)$, where $\Delta\phi$ is the instantaneous phase difference between the beams (referred to π).

Rather than fitting $N_{obs}(t)$ by $N_{model}(t)$ during a given few minutes long sequence, we fit the observed *distribution* of null values by the expected distribution of N_{model} values. The observable extracted from a given PFN chopped sequence is then the distribution of the measured null values $N_{obs}(t)$. The key advantage of this approach is that although none of the instantaneous dI, I_P and dark terms of Eq (8) are actually measured, their distributions can be accurately derived using the I_1, I_2, and Dark values recorded at slightly different times inside the sequence (see also Hanot et al. in these proceedings). In practice, if $P_{obs}(N_i)$ is the observed null probability density around null value N_i and $P_{model}(N_i)$ is the theoretical one, one performs a goodness of fit test by forming the Pearson χ^2 quantity:

$$Q = \sum_i \frac{(P_{obs}(N_i) - P_{model}(N_i))^2}{P_{model}(N_i)} \quad (10)$$

The only major assumption made in our modeling is that the differential phase has a Gaussian distribution, which is in good agreement with studies of residual phase after AO correction.[14] The only parameters of the model distribution which are not directly derived from the chopped data are then the astrophysical null depth N^{as} and the differential phase mean and rms values. For each value of these three parameters, one generates a null sequence $N_{model}(t)$ and computes the corresponding histogram. The parameters and error bars are then found by minimizing the reduced χ^2 = Q / (M-4), where M is the number of bins in the histogram). A typical null sequence, and the result of such a histogram fit are shown in figure 5 in the case of the giant star β Peg.

The agreement between the observed and best fit modeled distributions is generally excellent, with reduced χ^2 consistently around unity for all observations reported. This makes us confident that the modeling approach is sound. In addition, when several sequences are acquired for a given star and baseline orientation (case of α Boo, fig. 6), the derived null depths are extremely reproducible: at the 0.1% rms level or better. This is even true under changing observing conditions, e.g. apparent fluctuations of mean differential phase or overall seeing quality. This shows that the statistical null analysis method allows robust and accurate "self-calibration" of the data: no calibrator star is needed down to the 0.1% rms null accuracy or better. We therefore call this method "null self-calibration" or NSC. A more complete discussion of this post-processing method's principle, ultimate performance and general implications will be given in forthcoming papers (Hanot et al. in prep, Mennesson et al. in prep.)

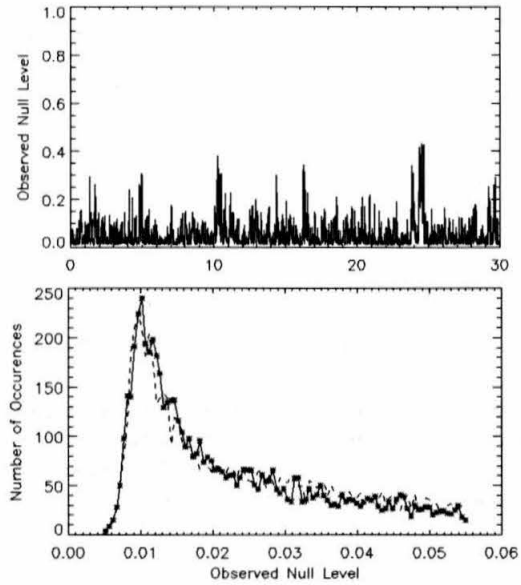

Figure 5. Top: null sequence obtained on β Peg (typical results, July 2009). Bottom, plain curve: observed null histogram. Bottom: dashed curve: best fit model null histogram. The best fit parameters are: $N^{as} = 0.0089 \pm 0.0004$, mean differential phase = 0.29 radian, differential phase rms = 0.48 radian.

4. RESULTS AND INTERPRETATION

Astrophysical nulls were measured with the PFN on nine stars over five nights: July 21 2008, November 11 & 12 2008, and July 10 & 11 2009. The 2009 data were obtained with an upgraded angle tracking camera and an achromatic beam recombination system, providing better null accuracy (typically 0.1% rms or better). As discussed in the previous section, some engineering parameters can also be derived from the observed null distributions, in particular the residual phase jitter after AO correction. The derived K band phase jitter ranges from 0.3 radian ($\simeq$ 100 nm) rms under good seeing conditions (July 2009) to 0.6 radian ($\simeq$ 200nm) rms under bad seeing conditions (November 2008). Taking into account the spatial averaging of the phase in each sub-aperture, these figures are well aligned with the AO performance which predicts a typical residual wavefront rms error of 200 to 250 nm over the full telescope aperture.

Various types of astronomical test observations were carried out: resolved giant stars already well characterized by long baseline interferometry, binary systems with known orbital parameters and flux ratios, and unresolved stars with possible excess emission. Fig. 6 compares the stellar nulls measured by the PFN to the values expected from near IR long baseline interferometric measurements of the stellar photospheres. The agreement is excellent for standard giants and supergiants (α Boo, α Her, β And), and for the binary system α Aur. Conversely, significant departure from naked photosphere models is detected for three of the variable mass losing stars: α Ori, ρ Per and χ Cyg. These measurements will be analyzed thoroughly in a forthcoming publication (Mennesson et al. in prep.). We only summarize hereafter the results obtained on three of the targets, illustrating instrumental performance in terms of null depth and accuracy (i.e. contrast).

For all stars, the expected null values are computed using equation 9, relating the astrophysical null depth N^{as} to the object's visibility V at the PFN's baseline B and effective wavelength λ:

$$V(\lambda) = \frac{\int I(\vec{\theta}) e^{j.2\pi \vec{B}.\vec{\theta}/\lambda} d\vec{\theta}}{\int I(\vec{\theta}) d\vec{\theta}} \tag{11}$$

$I(\vec{\theta})$ is the source brightness distribution at a wavelength λ, including the lobe antenna of the fiber. The baseline B corresponds to the center to center distance between the two elliptical 1.5 x 3m sub-apertures of the

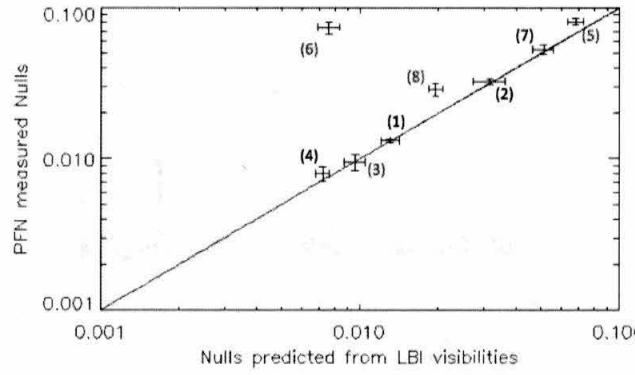

Figure 6. Stellar nulls measured by the Palomar Fiber Nuller compared to values expected from near IR long baseline interferometry (LBI) and stellar modeling (photosphere only). (1): α Boo,[15,16] (2): α Her,[17] (3): β Peg,[18] (4): β And,[19] (5): α Ori,[17] (6): ρ Per,[19] (7): α Aur,[20,21] (8): χ Cyg.[22] Departure from naked photosphere models is found for three of the Miras and semi-regular variable stars (red): α Ori, ρ Per and χ Cyg.

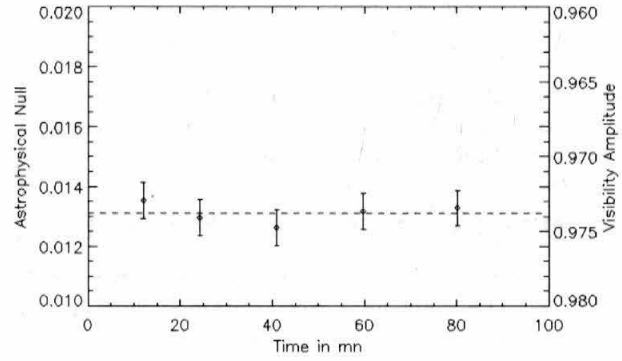

Figure 7. Astrophysical null depth (left vertical axis) and corresponding object's visibility (right vertical axis) measured as a function of time for α Boo. No calibrator star is used, visibilities are derived using the null self-calibration technique. All individual null error bars are below 0.0006, overall astrophysical null estimate is 0.0132 $\pm$ 0.0003, or equivalently V= 0.9739 $\pm$ 0.0006. The dashed line indicates the expected null depth (or visibility) at the PFN 3.4 m baseline, using α Boo's limb darkening model derived by long baseline interferometry.[15]

primary 5m diameter mirror. Based on the optical model of the telescope and on engineering data, the derived PFN interferometric baseline is 3.40 m $\pm$ 0.085m. Observations are made in a waveband covering 2.05 to 2.35 microns. Given the detector chromatic efficiency and the K-band filter transmission curve, the effective (center) wavelength of the PFN is determined to be 2.16 microns. The effective wavelength exhibits very small variations (<3nm) versus stellar temperature, and is assumed constant for all stars considered here.

4.1 α Boo

Figure 7 shows a series of five consecutive null (or equivalently visibility) measurements obtained on α Boo over a period of an hour, illustrating the accuracy of the NSC data processing, and the stability of the measurements. The astrophysical null depth derived for α Boo, using no calibrator observations, is 1.32% $\pm$ 0.03%.

The most accurate long baseline interferometric observations of α Boo determine a limb darkening diameter of 20.91 mas $\pm$ 0.08 mas,[15,16] and an effective temperature of 4300 K. They also conclude that no strong photometric asymmetry or bright stellar companion is present in the immediate stellar environment ($\simeq$ 1 AU). Using the 0.350 linear limb darkening coefficient predicted in the K band[23] for a 4300K giant star with log g =2.0, and equation (9) above, α Boo's expected astrophysical null depth is 1.31% $\pm$ 0.07% at the PFN baseline, in excellent agreement with the observed value. The PFN null uncertainty of 3 x 10^{-4} translates into an upper (3-sigma) limit of

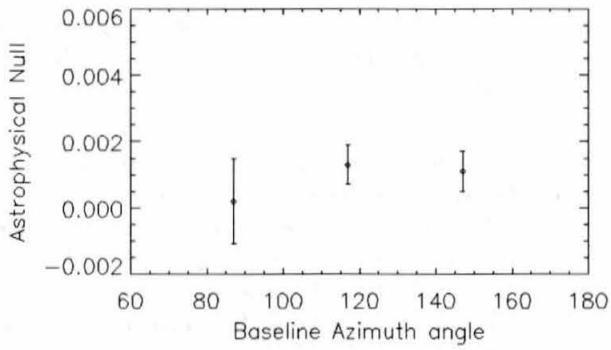

Figure 8. Astrophysical null depths measured on Vega for three different baseline orientations, using the NSC data reduction method. Measured nulls are largely below 0.01, with individual error bars of the order of 0.001 or lower. The baseline-averaged null depth is 0.0011 +/- 0.0006. These measurements place new upper limits to the flux contributed by potential sources of extra emission in the inner 0.2 to 2 AU region around Vega (Mennesson et al. in prep).

2 x 10^{-3} on the K band relative brightness of a companion located 35 to 100 mas away (along the baseline direction, see figure 1), i.e. between 0.4 AU and 1.1 AU at α Boo's distance. This limit is comparable to the 8 x 10^{-4} companion brightness upper limit derived at 1 AU from H-band visibility and phase closure measurements using the IOTA 3 telescope interferometer.[16] However, the IOTA measurements synthesized a total aperture size of 35 x 15 m., i.e. much larger than the Palomar 5m telescope. This illustrates the point that accurate null measurements do not only provide better contrast. They also provide better spatial resolution for a given baseline since smaller sources can be reliably resolved.

4.2 Vega

Fig 8 summarizes observations of Vega conducted on July 10 2009 under good seeing conditions, providing accurate null measurements over three baseline orientations spanning 60 degrees in azimuth. The orientation averaged null depth is 0.0011 +/- 0.0006, illustrating the PFN's ability to measure accurate deep nulls at the 0.001 level. In comparison, the expected null depth from Vega's latest photosphere model[24] is 0.0004. These early PFN measurements already strongly constrain the maximum level of emission due to various potential sources of extra emission in Vega's immediate vicinity (Mennesson et al. in prep).

4.3 ρ Per

ρ Per is an M4II semi-regular variable star with an effective temperature of $\simeq$ 3500 K and log g =0.8, yielding an estimated limb darkening K band coefficient of 0.394.[23] Using the measured limb darkened diameter of 16.04 mas $\pm$ 0.5 mas[19] and equation (9), the expected null depth is 0.76% $\pm$ 0.05%. Conversely, the observed value is 7.4% $\pm$ 0.7%, pointing to the largest excess among the stars in our sample, and suggesting a recent significant mass loss event since the measurements reported by Richichi et al.[19] More observations are required to constrain the source of extra emission, but extended outer molecular layers are expected around this kind of semi-regular M giants and could be responsible for the observed excess.

5. CONCLUSIONS

Accurate nulling ground-based measurements have so far been limited to the mid-infrared, where one can take advantage of the reduced turbulence and improved wavefront quality. Using a first generation low cost interferometric coronagraph and a dedicated data reduction algorithm, we have obtained high contrast (better than 0.1%) stellar observations in the near infrared, well within the diffraction limit of the Palomar 200 inch telescope. This demonstrates that although shorter wavelengths have higher phase fluctuations, high contrast interferometry is also possible in the near infrared, providing higher spatial resolution and much higher sensitivity from the ground. With the new PALM-3000 extreme AO system[26] coming on-line at Palomar in 2011, simulations

indicate that contrasts of the order of 10^{-4} to 10^{-3} should be readily accessible on $m_K = 6$ stars well within the diffraction limit of the full telescope. The fiber nuller observing and post processing approach can in principle be extended to long baseline interferometers using single-mode fibers for recombination, as long as a fringe tracker with standard performance ($\simeq$ 200 nm rms) and some dispersion capability are available (Mennesson et al. in prep).

A variety of astrophysical fields will generally benefit from this approach. Improved interferometric measurement accuracy helps distinguish between competing models, describing for instance the inner regions of protoplanetary disks or the central brightness distribution of active galactic nuclei. However, the most significant and straight forward contributions seem to be in the direct detection of debris disks hot counter parts and massive young planets around nearby (< 100 pc) stars. Because of contrast limitations at high angular resolution, successful direct observations of these faint objects have so far been restricted to the outer (> 10AU) regions of the circumstellar environment. Combined to the tenfold improvement in dynamic range gain, near infrared measurements over 0.1 to 10 AU spatial scales will provide observations of the terrestrial planet forming region at unprecedented contrast levels. In the case of young systems, they will help constrain the early dynamical process of disk / planets interaction, such as tidal migration, planet destruction, ejection of planetesimals and the overall role of massive planets in the evolution of debris disks. As for older debris disks, their inner brightness distribution reflects present dust sources (comets, asteroids), as well as past sinks (Poynting-Robertson drag, radiation pressure), and perturbations (collisions, evaporation, planets) sources, revealing some of the system formation's history.

Finally, when used on a single telescope, a fiber nuller system could be fed by an optical stop reflecting the very central part of the field (e.g. inner 3 λ/D) and hence work in conjunction with a regular coronagraph.

REFERENCES

[1] Liu, M.C. et al. 2009, AIP Conference Proceedings, 1094, 461
[2] Hinkley, S. et al. 2007, ApJ, 654, 633
[3] Boccalletti, A. et al. 2004, PASP, 116, 1061
[4] Serabyn, E. et al. 2010, Nature, 464, 1018
[5] Boccalletti, A. et al. 2008, SPIE Conf. Ser. 7015, ed. N. Hubin, C. Max, P. L. Wizinowich, 177
[6] Marois, C.et al. 2008, SPIE Conf. Ser. 7015, ed. N. Hubin, C. Max, P. L. Wizinowich, 47
[7] Kloppenborg, B. et al. 2010, Nature, 464, 870
[8] Haguenauer, P. & Serabyn, E. 2006, Applied Optics, 45, 2749
[9] Mennesson, B. et al. 2006, in SPIE Conf. Ser. 6268, Advances in Stellar Interferometry, ed. J.D. Monnier, M. Scholler, W.C. Danchi, 95
[10] Martin, S. et al. 2008, in SPIE Conf. Ser. 7013, Optical and Infrared Interferometry, ed. M. Scholler, W.C. Danchi, F. Delplancke, 57
[11] Mennesson, B. et al. 2002a, JOSA A, 19, 596
[12] Troy, M. et al. 2000, SPIE Conf. Ser. 4007, Adaptive Optical Systems Technology, ed. P. Wizinowich, 31
[13] Mennesson B. et al. 2003, in Proceedings of the Conference on Towards Other Earths: DARWIN/TPF and the Search for Extrasolar Terrestrial Planets, ed. M. Fridlund, T. Henning, 525
[14] Cagigal, M.P. & Canales, V. F. 2000, JOSA A, 17, 1318
[15] Perrin, G. et al. 1998, A&A, 331, 619
[16] Lacour, S. et al. 2008, A&A, 485, 561
[17] Perrin, G. et al. 2004, A&A, 418, 675
[18] Di Benedetto, G.P. & Rabbia, Y. 1987, A&A, 188, 114
[19] Richichi, A. et al. 2005, A&A, 431, 773
[20] Torres, G. et al. 2009, ApJ, 700, 1349
[21] Hartkopf, W. I. & Mason, B. D., Sixth Catalog of Orbits of Visual Binary Stars, USNO, Washington, DC.
[22] Lacour, S. et al. 2009, ApJ, 707, 632
[23] Claret, A. et al. 1995, A&AS, 114, 247
[24] Aufdenberg, J.P. et al. 2006, ApJ 645, 664
[25] Tsuji, T. 2001, A&A, 376, L1
[26] Bouchez, A. et al. 2008, 2008, SPIE Conf. Ser. 7015, ed. N. Hubin, C. Max, P. L. Wizinowich, 24

ACKNOWLEDGMENTS

This work was performed at the Jet Propulsion Laboratory, California Institute of Technology, under contract with NASA. We wish to thank the Palomar Observatory staff for their assistance in mounting the PFN and conducting the observations at the Hale telescope.